Arabian Journal of Chemistry (2017) **10**, S814–S824

King Saud University

Arabian Journal of Chemistry

www.ksu.edu.sa
www.sciencedirect.com

ORIGINAL ARTICLE

Mechanism investigation of the reaction between triphenylphosphine, dialkyl acetylenedicarboxylates and 2-hydroxybenzimidazole: Experimental and theoretical study

M. Zakarianezhad [a], **S.M. Habibi-Khorassani** [b,*], **M.T. Maghsoodlou** [b],
H. Ghasempour [c], **B. Makiabadi** [d]

[a] *Department of Chemistry, Payam Noor University, Tehran, Iran*
[b] *Department of Chemistry, The University of Sistan and Baluchestan, Zahedan, Iran*
[c] *Department of Chemistry, Bardsir Branch, Islamic Azad University, Bardsir, Iran*
[d] *Department of Chemical Engineering, Sirjan University of Technology, Sirjan, Iran*

Received 30 April 2012; accepted 15 December 2012
Available online 28 December 2012

KEYWORDS

Stable phosphorus ylides;
Kinetic study;
Z and *E* rotamers;
AIM analysis

Abstract In the recent work, NMR study and the stability of the *Z*- and the *E*- isomers were undertaken for the two rotational isomers of phosphorus ylides involving 2-hydroxybenzimidazole [namely dimethyl-2-(2-hydroxybenzimidazole-n-yl)-3-(triphenylphosp hanylidene) succinate] by natural population analysis (NPA) and atoms in molecules (AIM) methods. Quantum mechanical calculation was clarified how the ylides exist in solution as a mixture of the two geometrical isomers (*Z*- and *E*-) as a minor or major form. In addition, Kinetic studies were performed for the reaction between triphenylphosphine and dialkyl acetylenedicarboxilate in the presence of NH– heterocyclic compound, such as 2-hydroxybenzimidazole. To determine the kinetic parameters of the reaction, it was monitored by UV spectrophotometry. Useful information was obtained from studies of the effect of solvent and concentration of reactants on the rate of reaction. Proposed mechanism was confirmed according to the obtained results and steady state approximation and first step (k_2)

---

[*] Corresponding author. Address: Department of chemistry, The University of Sistan and Baluchestan, P.O. Box 98135-674, Zahedan, Iran. Tel./fax: +98 5412446565.
E-mail address: habibi_khorassani@yahoo.com (S.M. Habibi-Khorassani).

Peer review under responsibility of King Saud University.

Production and hosting by Elsevier

http://dx.doi.org/10.1016/j.arabjc.2012.12.012

and third step of reaction were recognized as a rate determining step and fast step, respectively on the basis of experimental data.

1. Introduction

Organophosphorus compounds have emerged as important reagents and intermediates in organic synthesis (Crayson and Griffith, 1972). An important group of this class is phosphorus ylides, which have been used in many reactions and synthesis of organic compounds (Hudson, 1990; Engel, 1988; Cadogan, 1979; Kalantari et al., 2006; Islami et al., 2005; Maghsoodlou et al., 2007; Anary-Abbasineja et al., 2008). The prominent role of these compounds is to convert the carbonyl groups to carbon–carbon double bonds (Maryanoff et al., 1989) from the large number of methods available for the synthesis of phosphorus ylides, the most important involve the reaction of a phosphonium salt with a base (Fitjer and Quabeck, 1985; Yavari et al., 2007). In recent years a method has been developed for the preparation of this family by using a novel approach employing vinyl phosphonium salts (Ramazan and Souldozi, 2005; Yavar and Alizadeh, 2003). The phosphonium salts are most often converted to the ylides by treatment with a strong base, though weaker bases can be used if the salt is acidic enough. Michael addition of phosphorus (III) compounds such as triphenylphosphine to acetylenic esters leads to reactive 1, 3-dipolar intermediate betaines which are not detected even at low temperature (Ramazani and Bodaghi, 2000). These unstable species can be trapped by a protic reagent, ZH, such as methanol, amide, imide, etc. to produce various compounds e.g. ylides (Hassanabad et al., 2009; Anaraki-Ardakan et al., 2008; Yavari et al., 2002;Wang et al., 2001; Islam et al., 2003; Yavari et al., 2006; Maghsoodlou et al., 2006a,b; Habibi-Khorassani et al., 2007; Habibi-khorassani et al., 2009).

These ylides usually exist as a mixture of the two geometrical isomers, although some ylides exhibit one geometrical isomer. Assignment of the stability of the two *Z*- and *E*-isomers is impossible in phosphorus ylides by experimental methods such as ^{1}H and ^{13}C NMR and IR spectroscopes, mass spectrometry and elemental analysis data. For this reason quantum mechanical calculation has been performed in order to gain a better understanding of the most important geometrical parameters and also relative energies of both the geometrical isomers.

2. Materials and methods

Quantum mechanical calculation has been performed by Gaussian98 program and using the AIM2000 program packages. Dialkyl acetylenedicarboxilate, triphenylphosphine and 2-hydroxybenzimidazole were purchased from Fulka (Buchs, Switzerland) and used without further purification. All extra pure solvents including 1, 2-dichloroethane and ethyl acetate also obtained from Merk (Darmstadt, Germany). A Cary UV/Vis spectrophotometer model Bio-300 with a quartz cell with 10 mm light-path was employed throughout the current work.

3. Results and discussion

3.1. Calculations

A facile synthesis of the reaction between triphenylphosphine **1**, dialkyl acetylenedicarboxylates **2** and 2-hydroxybenzimidazole **3** (as a NH– heterocyclic compound) for the generation of phosphorus ylides **4a**–**c** involving the two geometrical isomers such as *Z*- and *E*-isomers has been earlier reported (Maghsoodlou et al., 2006a,b). The reaction is shown in Fig. 1. For assignment of the two *Z*- and *E*-isomers as a minor or major form in phosphorus ylides **4a**–**b** containing 2-hydroxybenzimidazole, first the *Z*- and the *E*-isomers were optimized for all ylide structures at HF/6–31G(d,p) level of theory by Gaussian98 package program (Frisch et al., 1998). The relative stabilization energies in both the geometrical isomers have been calculated at HF/6–31G(d,p) and B3LYP/6–311++G(d,p) level of theory. Atoms in molecules (AIM) (Bader, 1990), natural population analysis (NPA) methods and CHelpG keyword at HF/6–31G(d,p) level of theory have been employed in order to gain a better understanding of most geometrical parameters of both the *E*-**4(a, b)** and the *Z*-**4(a, b)** of phosphorus ylides. The numbers of critical points and intramolecular hydrogen bonds as well as the charge of atoms that constructed on the *Z*- and *E*-isomers have been recognized. The results altogether reveal the effective factors on stability of the *Z*- and the *E*-ylide isomers. In addition, J_{x-y}, the values of proton and carbon coupling constants and also chemical shifts (δ^{H}_{iso}, δ^{C}_{iso}) have been calculated at mentioned level using SPINSPIN keyword. The relative stabilization energies for the two [*Z*-**4(a, b)** and *E*-**4(a, b)**] isomers (see Figs. 2 and 3) are reported in Table 1, as can be seen, *E*-**4a**

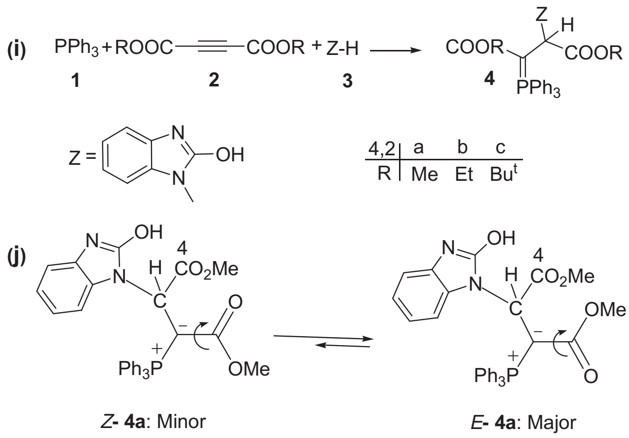

Figure 1 (**i**) The reaction between triphenylphosphine **1**, dialkyl acetylenedicarboxylate **2** (**2a** or **2b**) and 2-hydroxybenzimidazole **3** for generation of stable phosphorus ylides **4** (**4a** or **4b**), (**j**) The two rotational of isomers *E*-**4a** and *Z*-**4a** (major and minor, respectively) for ylide **4a**.

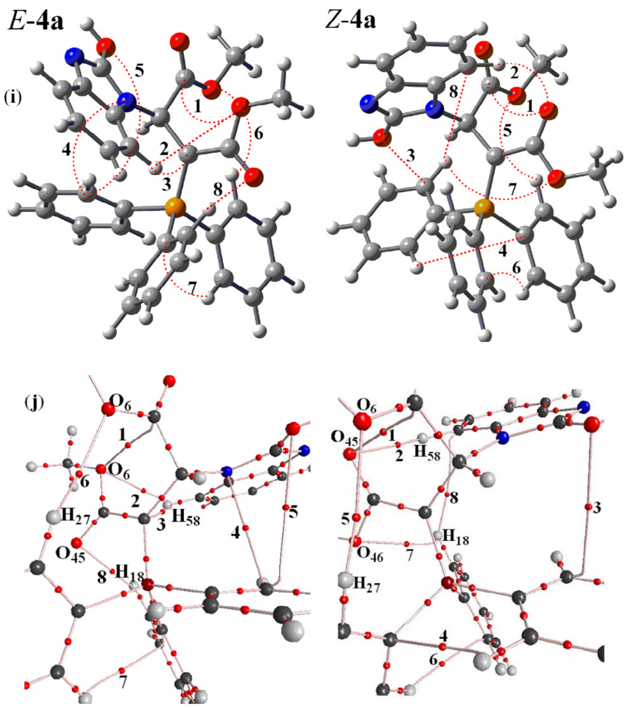

Figure 2 (**i**) Intramolecular hydrogen bonds (dotted lines) in the two *E*-**4a** and *Z*-**4a** geometrical isomers of stable ylide **4a**, (**j**) A Part of molecular graphs, including intramolecular hydrogen bond at critical points (BCPs) for the two rotational isomers such as *E*-**4a** and *Z*-**4a.** Small red spheres, and lines corresponding to BCPs bond paths, respectively.

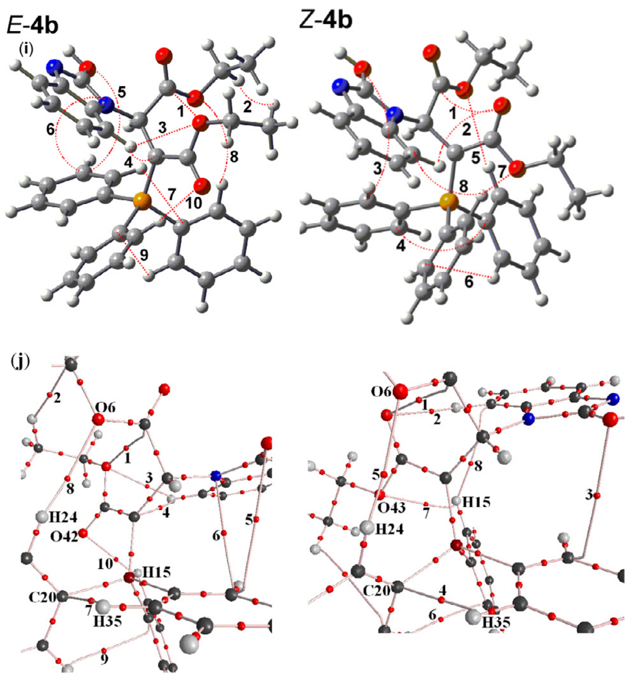

Figure 3 (**i**) Intramolecular hydrogen bonds (dotted lines) in the two *E*-**4b** and *Z*-**4b** geometrical isomers of stable ylide **4b**, (**j**) A Part of molecular graphs, including intramolecular hydrogen bond at critical points (BCPs) for the two rotational isomers such as *E*-**4b** and *Z*-**4b**. Small red spheres, and lines corresponding to BCPs bond paths, respectively.

and *Z*-**4b** isomers are more stable than *Z*-**4a** and *E*-**4b** forms (0.41 and 0.18 kcal/mol, respectively) at B3LYP level of theory.

Further investigation was undertaken in order to determine more effective factors on the stability of the two *Z*- and *E*-isomers on the basis of AIM calculations at HF/6–31G(d,p) level of theory by the AIM2000 program package (Biegler Konig et al., 2001). In recent years, AIM theory has often been applied in the analysis of H-bonds. In this theory, the topological properties of the electron density distribution are derived from the gradient vector field of the electron density $\nabla\rho(\underline{r})$ and from the Laplacian of the electron density $\nabla^2\rho(r)$. The Laplacian of the electron density, $\nabla^2\rho(r)$, identifies regions of space wherein the electronic charge is locally depleted $[\nabla^2\rho(r) > 0]$ or built up $[\nabla^2\rho(r) < 0]$ (Bader, 1990). Two interacting atoms in a molecule form a critical point in the electron density, where $\nabla\rho(r) = 0$, called the bond critical point (BCP). The values of the charge density and its Laplacian at these critical points give useful information regarding the strength of the H-bonds. The ranges of $\rho(r)$ and $\nabla^2\rho(r)$ are $0.002 - 0.035e/a_0^3$ and $0.024–0.139e/a_0^5$, respectively, if H-bonds exist (Grabowsk, 2001). The AIM calculation indicates intramolecular hydrogen bond critical points (H-BCP) for the two *Z*-**4**(**a**, **b**) and *E*-**4**(**a**, **b**) isomers. Intramolecular H-BCPs along with a part of molecular graphs for the two rotational isomers are shown in Figs. 2 and 3 (dotted line). Most important geometrical parameters involving some H-bonds (bond length and their relevant bond angle) are reported in Table 2. The electron density $(\rho) \times 10^3$, Laplacian of electron density $\nabla^2\rho(r) \times 10^3$, and energy density $-H(r) \times 10^4$ are also reported in Tables 3 and 4. A negative total energy density at the BCP reflects a dominance of potential energy density, which is the consequence of accumulated stabilizing electronic charge (Arnol and Oldfield, 2000). Herein, the number of hydrogen bonds in both categories (*E*-**4a** and *Z*-**4a**) and (*E*-**4b** and *Z*-**4b**) are (8 and 8) and also (10 and 8), respectively. The values of ρ and $\nabla^2\rho(r) \times 10^3$ for those are in the ranges (0.002 – 0.014 and 0.003 – 0.014 $e/a_0{}^3$) and (0.002 – 0.014 and 0.003 – $0.014e/a_0^3$) and also (12.35 – 61.89 and 10.29 – $56.88e/a_0^5$) and (8.06 – 59.91 and 10.48 – $57.15e/a_0^5$), respectively. In addition, the Hamiltonian $[-H(r) \times 10^4]$ are in the ranges (5.78 – 15.09 and 5.79 – 17.16 au) and (5.01 – 18.51 and 5.72 – 17.06 au), respectively (see Tables 3 and 4). These HBs show $\nabla^2\rho(r) > 0$ and $H(r) < 0$, which according to the classification of (Rozas et al., 2000) are medium-strength hydrogen bonds. In both ylides the dipole moment for the two *E*-**4a** and *E*-**4b** isomers (7.68 and 7.43 D) is smaller than the two *Z*-**4a** and *Z*-**4b** isomers (10.76 and 10.18 D, respectively) and the value of $-H_{tot}$ $(=\Sigma -H(r) \times 10^4)$ for the two *E*-**4a** and *Z*-**4b** isomers (84.47

Table 1 The relative energy (kcal/mol) for both the *Z*- and *E*-isomers of ylides **4a** and **4b**, obtained at HF/6–31G(d,p) and B3LYP/6–311 + + G(d,p) levels.

Geometrical isomer	HF	B3LYP
Z-4a	0.49	0.41
E-4a	0.00	0.00
Z-4b	0.004	0.00
E-4b	0.00	0.18

Table 2 Most important geometrical parameters corresponding to H-bonds (bond lengths and their relevant angles) for the two *Z* and *E* isomers in both ylides **4a** and **4b**. Bond lengths in Angstroms and bond angles in degrees, respectively.

	E-**4a**	*Z*-**4a**	*E*-**4b**	*Z*-**4b**
$C_{55}H_{58}....O_{46(45)}$[c]	2.57[a] (132.48)[b]	2.39 (147.22)		
$C_{24}H_{27}....O_6$[d]	2.72 (169.18)	2.80 (165.25)		
$C_{14}H_{18}....O_{45(46)}$	2.31 (129.35)	2.61 (111.90)		
$C_{21}H_{24}....O_6$			2.76 (168.56)	2.82 (164.61)
$C_{11}H_{15}....O_{42(43)}$			2.32 (127.70)	2.67 (107.84)
$C_{32}H_{35}....C_{20}$			2.67 (107.84)	2.71 (106.39)

[a] Bond length.

[b] Bond angle.

[c] Is relevant to the *Z* isomer.

[d] Is relevant to the both *Z* and *E* isomers.

and 85.86 au) is smaller than the two *Z*-**4a** and *E*-**4b** isomers (96.10 and 104.31 au, respectively). Although, $-H_{tot}$ in the *E*-**4a** is lower than the *Z*-**4a** and appear as an effective factor on instability of the *E*-**4a**, but the values of dipole moment in the *E*-**4a** are less than *Z*-**4a** and considered as an important fact on stability of *E*-**4a**. The results are summarized in Table 5. This difference for the two isomers (*E*-**4b** and *Z*-**4b)** in ylide **4b** involving less dipole moment, large $-H_{tot}$ and more hydrogen bonds as three dominate factors on stability provides a good chance for *E*-**4b** isomer to be a major isomer. On the basis of theoretical calculations (Table 1), the *Z*-**4b** has a slight stability with respect to the *E*-**4b** (0.18 kcal/mol) isomers and seems to be different from the results of predictable properties of the most important geometrical parameters (Table 5). Perhaps, this slightly different behavior is relevant to the huge structures of the two ylides **4(a**, **b**) involving three large atoms such as the two nitrogen, four oxygen and phosphorus and the large number of other atoms (C and H). This point, made a limitation in application of basis set higher than B3LYP/6–311++G(d,p) for a higher performance to gain more accurate calculations. Nevertheless, the results emerging from the geometrical parameters (dipole moment, $-H_{tot}$ and number of hydrogen bonds) for the *E*-**4**(**a**, **b**) category, are compatible with the experiment results from the ^1H, ^{13}C, ^{31}P NMR spectroscopes [30] which indicate the two isomers of *E*-**4a** and *E*-**4b** with the experimental abundance percentage of 63% and 71% (major forms) with respect to the *Z*-**4**(**a**, **b**) (minor forms).

Also, the charge on different atoms which is calculated by AIM and NPA methods and also CHelpG keyword at HF/6–31G(d,p) level is reported in Table 6 for the two *Z*- and *E*-isomers of ylides **4a** and **4b**. There is a good agreement between the results in three methods.

The individual chemical shifts have been characterized by NMR calculations at mentioned level using SPINSPIN key-

Table 3 The values of $a = \rho \times 10^3$, $b = \nabla^2\rho \times 10^3$ and $c = -H(r) \times 10^4$ for both the *Z*-**4a** and *E*-**4a** isomers of ylide **4a** calculated at the hydrogen bond critical points. All quantities are in atomic units.

E	*a*	*b*	*c*	Z	*a*	*b*	*c*
1	14.76	61.89	14.09	1	14.06	56.88	13.21
2	8.15	32.63	10.66	2	11.34	39.02	5.79
3	7.72	26.86	12.36	3	4.52	16.43	6.53
4	5.55	18.11	5.78	4	9.20	34.94	17.16
5	2.96	12.35	6.24	5	4.35	18.75	9.39
6	5.15	21.28	9.16	6	9.44	32.98	14.49
7	8.89	31.41	15.09	7	8.50	35.13	13.07
8	14.05	49.75	5.95	8	3.07	10.29	6.06

Table 4 The values of $a = \rho \times 10^3$, $b = \nabla^2\rho \times 10^3$ and $c = -H(r)\times10^4$ for both the *Z*-**4b** and *E*-**4b** isomers of ylide **4b** calculated at the hydrogen bond critical points. All quantities are in atomic units.

E	*a*	*b*	*c*	*Z*	*a*	*b*	*c*
1	14.27	59.91	14.28	1	14.10	57.15	13.25
2	2.33	8.06	5.01	2	11.34	38.97	5.72
3	8.26	33.01	10.77	3	4.55	16.53	6.54
4	7.64	26.89	12.63	4	9.21	34.82	17.06
5	3.05	12.46	6.17	5	4.25	17.02	9.47
6	5.35	17.58	5.74	6	9.45	33.09	14.53
7	9.66	37.80	18.51	7	8.44	34.95	13.15
8	4.74	20.02	9.36	8	3.13	10.48	6.15
9	8.96	31.53	15.09				
10	13.69	49.03	6.76				

Table 5 The most important geometrical parameters involving the value of H_{tot}/au, dipole moment/D and the number of hydrogen bonds for the two *Z*- and *E*-isomers of ylides **4a** and **4b**.

Geometrical isomer	H_{tot}/au	Dipole moment/D	Number of hydrogen bond
E-4a	84.47	7.68	8
Z-4a	96.10	10.76	8
E-4b	104.31	7.43	10
Z-4b	85.86	10.18	8

word. The total spin–spin coupling constant is the sum of four components: the paramagnetic spin–orbit (PSO), diamagnetic spin–orbit (DSO), Fermi-contact (FC) and spin-dipole (SD) terms. The value of chemical shifts (δ) and coupling constants (J_{X-Y}) is reported in (Tables 7–10) for the two major *E*-**4**(**a, b**) and minor *Z*-**4**(**a, b**) geometrical isomers. As can be seen, there is good agreement between both the experimental (Maghsoodlou et al., 2006a,b) and theoretical chemical shifts (δ) and coupling constants (J_{X-Y}). In the present work, molecular structures of ylides **4a**–**b** involving three large atoms such as sulfur, phosphorus and nitrogen atoms are huge along with the large numbers of other atoms, for this reason, employment of higher level of theory with basis set higher than HF/6–311 + +G(d,p) is impossible for a higher performance to gain more accurate calculations. This limitation causes a small difference between both the experimental and theoretical coupling constants in some functional groups.

3.2. Kinetics studies

To gain further insight into the mechanism in the reaction between triphenylphosphine **1,** dialkyl acetylenedicarboxylates **2** and 2-hydroxybenzimidazole **3** (as a NH– heterocyclic compound) for generation of phosphorus ylids **4a**–**c**, a kinetics study of the reactions was undertaken by the UV spectrophotometric technique (Aitken et al., 2007; Nielsen et al., 1995; Dash et al., 2011). To find the appropriate wavelength to follow the kinetic study of the reaction, in the first experiment, 3×10^{-3} M solution of compounds **1, 2c** and **3** was prepared in 1, 2-dichloroethane as solvent and the relevant spectra were recorded over the wavelength range of 200–400 nm. Figs. 4–6 shows the ultraviolet spectra of compounds **1**, **2c** and **3** respectively. In a second experiment, a 1 mL aliquot from the 3×10^{-3} M solutions of each compound of **1** and **3** was pipetted first into a quartz spectrophotometer cell (as there is no reaction between them), later 1 mL aliquot of the 3×10^{-3} M solution of reactant **2c** was added to the mixture and the reaction monitored by recording scans of the entire spectra every 13 min over the whole reaction time in the presence of **1, 2c** and **3** at ambient temperature as shown in Fig. 7 is typical. From this, the appropriate wavelength was found to be 330 nm (corresponding mainly to product **4**). The UV–Vis spectra of compound **4c** were measured over the concentration range (2×10^{-4} M $\leqslant M_{4c} \leqslant 10^{-3}$ M) to check for a linear relationship between absorbance values and concentrations. With the suitable concentration range and wavelength identified, the following procedure was employed.

Table 6 The charges on different atoms for the two *E* and *Z* isomers in both ylides **4a** and **4b,** calculated at HF/6–31G(d,p) theoretical level.

Number of atom	*Z*-**4a**	*E*-**4a**	*Z*-**4b**	*E*-**4b**
C1[d]	1.84[a]	1.84	1.86	1.86
	0.95[b]	0.95	0.96	0.95
	0.87[c]	0.86	0.85	0.86
C2	-7.79×10^{-1}	-7.79×10^{-1}	-7.80×10^{-1}	-8.09×10^{-1}
	−0.89	−0.88	−0.89	−0.88
	−0.68	−0.66	−0.66	−0.66
C3	7.36×10^{-1}	7.34×10^{-1}	7.36×10^{-1}	7.32×10^{-1}
	−0.10	−0.10	−0.09	−0.10
	0.72	0.45	0.64	0.60
O45(42)[e]	−1.40	−1.40	−1.40	−1.41
	−0.77	−0.80	−0.77	−0.80
	−0.64	−0.70	−0.65	−0.68
O46(43)	−1.28	−1.27	−1.31	−1.29
	−0.66	−0.64	−0.67	−0.65
	−0.41	−0.35	−0.44	−0.44
P11(8)	3.23	3.23	3.24	3.24
	1.87	1.87	1.87	1.87
	0.15	0.23	0.21	0.19

[a] Calculated by the AIM method.

[b] Calculated by the NPA method.

[c] Calculated by CHelpG keyword.

[d] Is relevant to the both 4a and **4b** ylides.

[e] Is relevant to ylide **4**.

Table 7 Selected ^1H NMR chemical shift (δ in ppm) and coupling constants (J in Hz) for some functional groups in the *E*-**4a** isomer as a major form.

Groups	δ^H/ppm	J_{PH}/Hz
6H, 2s, 2 CO_2Me	3.16[a] (3.51)[b] 3.79 (3.80)	
19H, m, $3C_6H_5$ and $C_7H_4N_2$	6.96–7.78 (7.14–7.80)	
1H, d, *P* = C–CH	5.32 (3.96)	16.40[a] (17.80)[b]

[a] Experimental data in accord with the results reported in the literature.
[b] Theoretical data.

For each kinetic experiment, the reaction kinetics was followed by plotting UV absorbance against time at 12.0 °C in 1,2-dichloroethane. Fig. 8 shows the absorbance change (dotted line) versus time for the 1:1:1 addition reaction between compounds **1, 2c** and **3** at 12.0 °C. Using the original experimental absorbance versus time data provided a second-order fit curve (solid line) by the software associated with the UV instrument (Schwartz and Gelb, 1978) that fits exactly the experimental curve (dotted line) (Fig. 9). This result indicates that the reaction between triphenylphosphine **1**, di-*tert*-butyl acetylenedicarboxylate **2c** and **3** follows second-order kinetics. The second-order rate constant (k_2) is then automatically calculated using a standard equation (Schwartz and Gelb, 1978; Okubo et al., 1989) within the program at 12.0 °C. It is reported in Table 11.

Furthermore, kinetic studies were carried out in continuation of experiments with different concentrations (5×10^{-3} M and 7×10^{-3} M). As expected, the second-order rate constant was independent of concentration and its value was the same as in the previous experiment.

3.3. Effect of solvents and temperature

To determine the effect of change in temperature and solvent environment on the rate of reaction, it was elected to perform various experiments at different temperatures and solvent polarities but otherwise under the same conditions as for the previous experiment. For this purpose, ethyl acetate with dielectric constant six was chosen as a suitable solvent since it not only could dissolve all compounds but also did not react with them. The rate constant of the reaction in different solvents and temperatures is given in Table 11. The results show that the rate of reaction in each case was increased at higher temperature. In addition, the rate of reaction between **1**, **2c** and **3** was accelerated in a higher dielectric constant environment (1, 2-dichloroethane) in comparison with a lower dielectric constant environment (ethyl acetate) at all temperatures investigated. In the temperature range studied, the dependence of the second-order rate constant (ln k_2) on reciprocal temperature is consistent with the Arrhenius equation (Fig. 10), giving activation energy of reaction between **1**, **2c** and **3** from the slope (Table 12).

Table 8 Selected ^1H NMR chemical shift (δ in ppm) and coupling constants (J in Hz) for some functional groups in the *Z*-**4a** isomer as a minor form.

Groups	δ^H/ppm	J_{PH}/Hz
6H, 2s, 2 CO_2Me	3.70[a] (3.59)[b] 3.77 (3.67)	
19H, m, $3C_6H_5$ and $C_7H_4N_2$	6.96–7.78 (7.36–8.60)	
1H, d, *P* = C–CH	5.24 (4.16)	18.60[a] (15.23)[b]

[a] Experimental data in accord with the results reported in the literature.
[b] Theoretical data.

Table 9 Selected ^{13}C NMR chemical shift (δ in ppm) and coupling constants (J in Hz) for some functional groups in the *E*-**4a** isomer as a major form.

Groups	δ^C/ppm	J_{PC}/Hz
d, C_{ipso}	126.27[a] (126.62)[b]	91.60[a] (91.81)[b]
d, C_{para}	132.16 (132.67)	
d, *P* = C–CH	55.57 (53.31)	
d, C_{meta}	128.78 (126.59)	12.3 (8.74)
d, C_{ortho}	133.50 (134.22)	9.90 (13.62)
2s, 2OMe	49.32 (46.44) 52.63 (47.39)	
1C, $C_7H_4N_2$	155.03 (151.72)	
d, C^4 = O	169.62 (165.65)	12.60 (13.62)
P–C = C	171.71 (167.63)	
d, *P* = C	40.47 (33.11)	

[a] Experimental data in accord with the results reported in the literature.
[b] Theoretical data.

Table 10 Selected ^{13}C NMR chemical shift (δ in ppm) and coupling constants (J in Hz) for some functional groups in the *Z*-**4a** isomer as a minor form.

Groups	δ^C/ppm	J_{PC}/Hz
d, C_{para}	132.18[a] (132.37)[b]	
d, C_{ipso}	126.41 (126.45)	92.0[a] (90.15)[b]
d, C_{ortho}	133.58 (132.67)	10.20 (8.62)
d, C_{meta}	128.84 (126.68)	12.30 (10.82)
2s, 2OMe	50.38 (45.61) 52.39 (47.75)	
d, C^4 = O	170.23 (165.54)	15.80 (13.51)
d, *P* = C–CH	56.12 (52.38)	
1C, $C_7H_4N_2$	155.24 (150.97)	
d, *P*–C = C	171.91 (165.18)	
d, *P* = C	40.85 (31.70)	

[a] Experimental data in accord with the results reported in the literature.
[b] Theoretical data.

3.4. Effect of concentration

To determine the reaction order with respect to triphenylphosphine **1** and dialkyl acetylene-dicarboxylate **2** (**2c**), in continuation of experiments**,** all kinetic studies were carried out in the presence of excess **3**. Under this condition, the rate equation may therefore be expressed as:

$$rate = k_{obs}[1]^{\alpha}[2]^{\beta} \quad k_{obs} = k_2[3]^{\gamma} \quad \text{or} \quad ln\,k_{obs} = ln\,k_2 + \gamma\, ln \qquad (1)$$

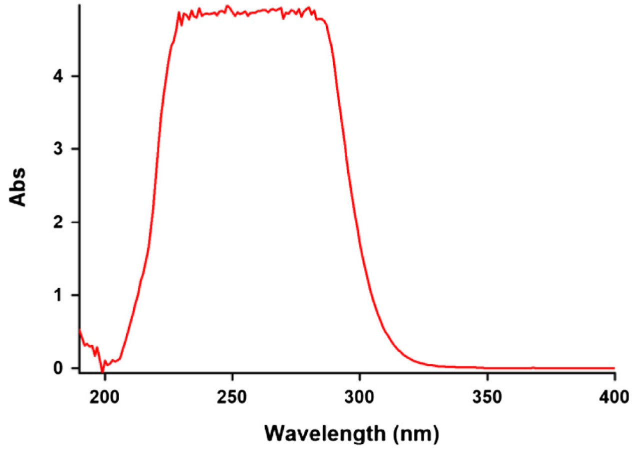

Figure 4 The UV spectrum of 10^{-3}M triphenylphosphine **1** in 1, 2-dichloroethane.

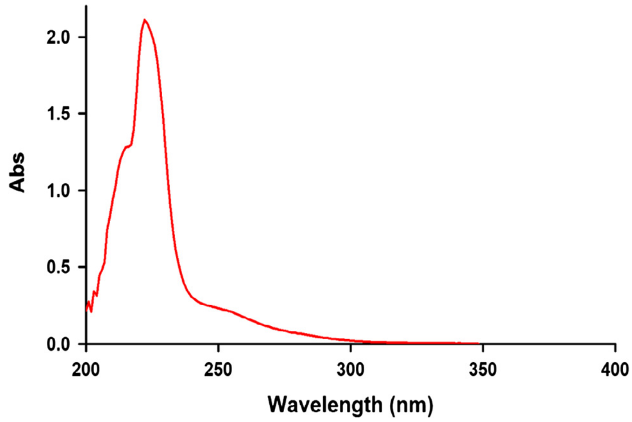

Figure 5 The UV spectrum of 10^{-3}M di-*tert*-butyl acetylenedicarboxylate **2c** in 1, 2-dichloroethane.

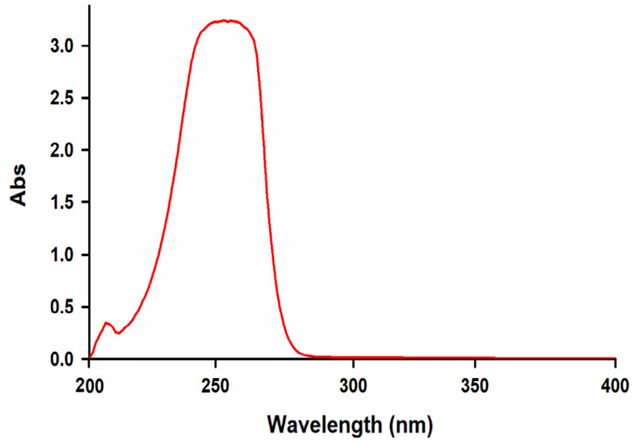

Figure 6 The UV spectrum of 10^{-3}M 2-hydroxybenzimidazole **3** in 1, 2-dichloroethane.

In this case (3×10^{-2} M of **3** instead of 3×10^{-3} M), second order fit curve (solid line) against time at 335 nm exactly fits to the original experimental absorbance versus time data. The value of rate constant was the same as that obtained from the previous experiment (3×10^{-3} M). Same results were obtained with repetition of the experiments in 5×10^{-2} M and 7×10^{-2} M of **3**. In fact, the experimental data indicated that the observed pseudo second order rate constant (k_{obs}) was equal to the second order rate constant (k_2), this is possible when γ is zero in Eq. (1) and the reaction is zero order with respect to **3** (NH-heterocyclic compound) and the sum of **1** and **2** (**2a**) ($\alpha + \beta = 2$), respectively.

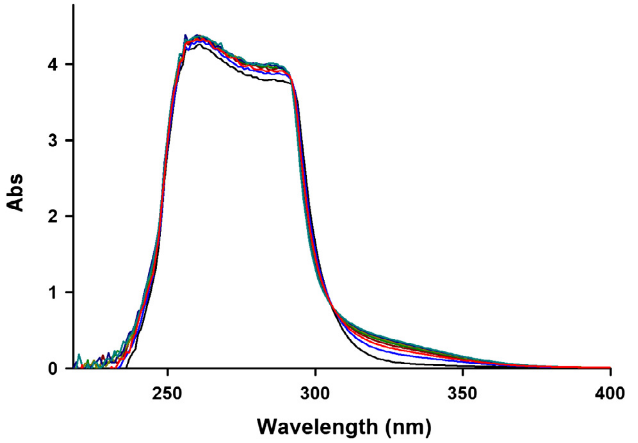

Figure 7 The UV spectra of the reaction between **1, 2c** and **3** with 10^{-3}M concentration of each compound as reaction proceeds in 1, 2-dichloroethane with 10 mm light-path cell for generation of **4** (**4c**).

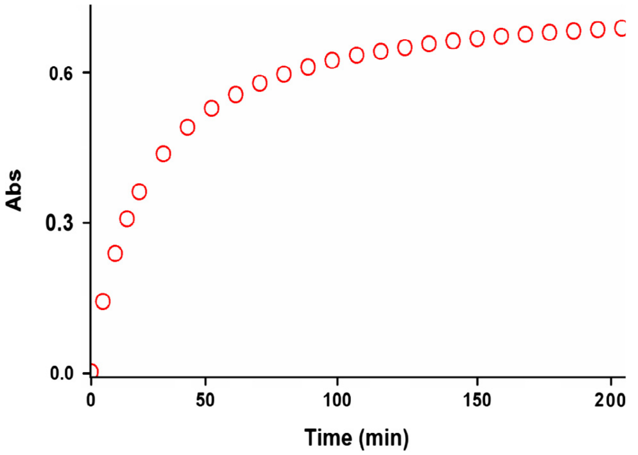

Figure 8 The experimental absorbance changes (dotted line) against time at 330 nm for the reaction between compounds **1, 2c** and **3** at 12.0 °C in 1, 2-dichloroethane.

To determine the reaction order with respect to dialkyl acetylenedicarboxylate **2** (**2c**), the continuation of experiment was performed in the presence of excess of **1** (rate $= k'_{obs}[3]^{\gamma}[2]^{\beta}$, $k'_{obs} = k_2[1]^{\alpha}(2)$). The original experimental absorbance versus time data provide a pseudo first order fit curve at 330 nm, which exactly fits the experimental curve (dotted line).

As a result since $\gamma = 0$ (as determined previously), it is reasonable to accept that the reaction is first order with respect to compound **2** (**2c**) ($\beta = 1$). Because the overall order of reaction is 2 ($\alpha + \beta + \gamma = 2$) it is obvious that $\alpha = 1$ and the reaction order with respect to triphenylphosphine **1** must be equal to

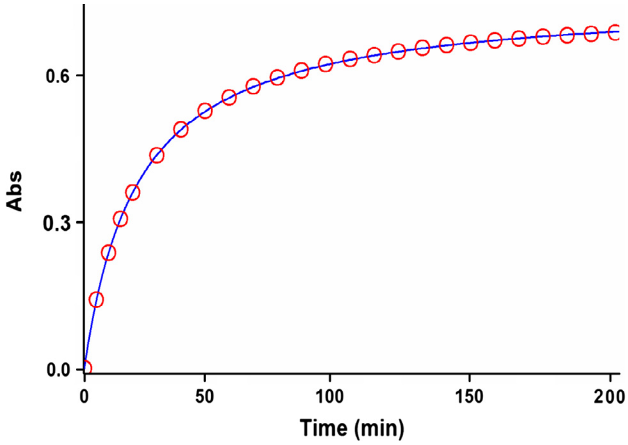

Figure 9 Second order fit curve (solid line) accompanied by the original experimental curve (dotted line) for the reaction between compounds **1, 2c** and **3** at 330 nm and 12.0 °C in 1, 2-dichloroethane.

one. This observation was obtained also for reactions between (**1, 2b** and **3**) and (1, **2a** and **3**) for generating **4b** and **4a**, respectively. Based on the above results, a simplified proposed reaction mechanism is shown in Fig. 11.

The experimental results indicate that the third step (rate constant k_3) is possibly fast. In contrast, it may be assumed that the third step is the rate determining step for the proposed mechanism. In this case the rate law can be expressed as follows:

$$rate = k_3[I_1][3] \tag{3}$$

The steady state assumption can be employed for $[I_1]$ which is generated by the following equation,

$$[I_1] = \frac{k_2[1][2]}{k_{-2} + k_3[3]}$$

The value of $[I_1]$ can be replaced in Eq. (3) to obtain this equation:

$$rate = \frac{k_2 k_3[1][2][3]}{k_{-2} + k_3[3]}$$

Since it was assumed that k_3 is relevant to the rate determining step, it is reasonable to make the following assumption: $k_{-2} \gg k_3\,[3]$

So the rate of low becomes:

$$rate = \frac{k_2 k_3[1][2][3]}{k_{-2}}$$

The final equation indicates that the overall order of reaction is three which is not compatible with experimental overall order of reaction (= two). In addition, according to this equation, the order of reaction with respect to 2-hydroxybenzimidazole **3** is one, whereas it was actually shown to be equal to zero. For this reason, it appeared that the third step is fast. If we assume that the fourth step (rate constant k_4) is the rate-determining step for the proposed mechanism, in this case, there are two ionic species to consider in the rate determining step, namely phosphonium ion (I_2) and 2-hydroxybenzimidazole (N^-). The phosphonium and 2-hydroxybenzimidazole ions, as we see in Fig. 11, have full positive and negative charges and form very powerful ion- dipole bonds to 1,2-dichloroethane, the high dielectric constant solvent. However, the transition state for the reaction between two ions carries a dispersed charge, which here is divided between the attacking 2-hydroxybenzimidazole and the phosphonium ions. Bonding of solvent (1, 2-dichloroethane) to this dispersed charge would be much weaker than to the concentrated charge of 2-hydroxybenzimidazole and phosphonium ions. The solvent thus stabilizes the species ions more than it would the transition state, and therefore E_a would be higher, slowing down the reaction. However, in practice, 1, 2-dichloroethane speeds up the reaction and for this reason, the fourth step, which is independent of the change in the solvent medium, could not be the rate determining step. Furthermore, the rate law of formation of the product (fourth step) for a proposed reaction mechanism with application of steady state assumption can be expressed by:

$$rate = k_4[I_2][N^-]$$

By application of steady state for $[I^-]$ and $[N^-]$, and replacement of their values in the above equation, the following equation is obtained:

$$rate = \frac{k_2 k_3[1][2][3]}{k_{-2} + k_3[3]} \tag{4}$$

This equation is independent of rate constant for the fourth step (k_4) and shows why the fourth step would not be affected by a change in the solvent medium. In addition, it has been suggested earlier that the kinetics of ionic species phenomena (e.g., the fourth step) are very fast (Okubo et al., 1989). If the first step (rate constant k_2) were the rate determining step, in this case, two reactants (triphenylphosphine **1** and dialkyl

Table 11 Values of overall second order rate constant for all reactions (**1**, **2c** and **3**), (**1**, **2b** and **3**) and (**1**, **2a** and **3**) in the presence of solvents such as 1, 2-dichloroethane and ethyl acetate, respectively, at all temperatures investigated.

Reaction	Solvent	k_2.M^{-1}.min^{-1}			
		12.0 °C	**17.0 °C**	**22.0 °C**	**27.0 °C**
1, **2c** and **3**	1,2-dichloroethane	48.4	63.1	82.2	106.6
	ethyl acetate	28.0	41.1	52.3	71.0
1, **2b** and **3**	1,2-dichloroethane	342.2	393.5	426.6	568.3
	ethyl acetate	197.0	250.0	296.1	370.8
1, **2a** and **3**	1,2-dichloroethane	578.2	657.6	732.2	854.5
	ethyl acetate	290.0	376.0	410.1	502.2

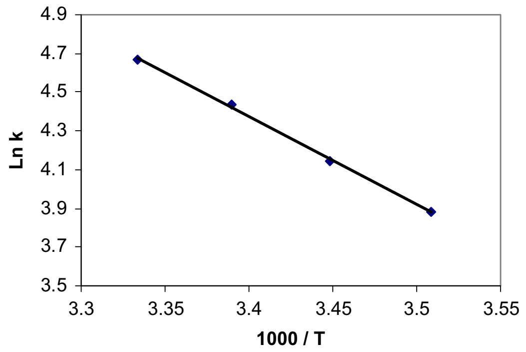

Figure 10 Dependence of second order rate constant (ln k_2) on reciprocal temperature for the reaction between compounds **1, 2c** and **3** for generating **4c** measured at wavelength 330 nm in 1, 2-dichloroethane in accordance with Arrhenius equation.

acetylenedicarboxylate **2**), as we see in Fig. 11, have no charge and could not form strong ion–dipole bonds to the high dielectric constant solvent, 1,2-dichloroethane. However, the transition state carries a dispersed charge which here is divided between the attacking **1** and **2** and, hence, bonding of solvent to this dispersed charge is much stronger than the reactants, which lack charge. The solvent thus stabilizes the transition state more than it does the reactants and, therefore, E_a is reduced which speeds up the reaction. Our experimental results show that the solvent with higher dielectric constant exerts a powerful effect on the rate of reaction (in fact, the first step has rate constant k_2 in the proposed mechanism) but the opposite occurs with the solvent of lower dielectric constant, (see Tables 11 and 12). The results of the current work (effects of solvent and concentration of compounds) have provided useful evidence for steps 1 (k_2), 3 (k_3) and 4 (k_4) of the reactions between triphenylphosphine **1**, dialkyl acetylenedicarboxylate **2** (**2a, 2b** or **2c**) and 2-hydroxybenzimidazole **3**. Two steps involving 3 and 4 are not determining, although the discussed effects, taken altogether, are compatible with the first step (k_2) of the proposed mechanism and would allow it to be the rate-determining step. However, a good kinetic description of the experimental result using a mechanistic scheme based upon the steady state approximation is frequently taken as evidence of its validity. By application of this, the rate formation of product **4** from the reaction mechanism (Fig. 11) is given by:

$$\frac{d[4]}{dt} = \frac{d[ylide]}{dt} = rate = k_4[I_2][N^-] \tag{5}$$

We can apply the steady-state approximation to $[I_1]$ and $[I_2]$;

$$\frac{d[I_1]}{dt} = k_2[1][2] - k_{-2}[I_1] - k_3[I_1][3],$$

$$\frac{d[I_2]}{dt} = k_3[I_1][3] - k_4[I_2][N^-]$$

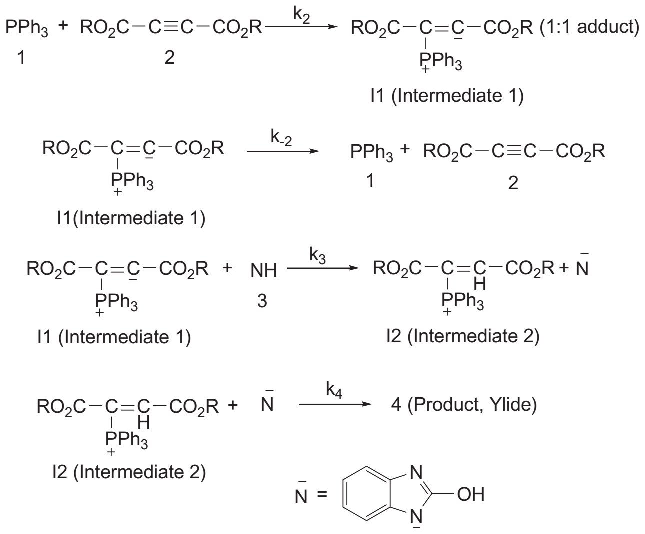

Figure 11 Proposed mechanism for the reaction between **1, 2** (**2a**, **2b** or **2c**) and **3** for generation of phosphorus ylides **4a–c**.

To obtain a suitable expression for $[I_2]$ to put into Eq. (5) we can assume that, after an initial brief period, the concentration of $[I_1]$ and $[I_2]$ achieves a steady state with their rates of formation and rates of disappearance just balanced. Therefore $\frac{d[I_1]}{dt}$ and $\frac{d[I_2]}{dt}$ are zero and we can obtain expressions for $[I_2]$ and $[I_1]$ as follows:

$$\frac{d[I_2]}{dt} = 0, \quad [I_2] = \frac{k_3[I_1][3]}{k_4[N^-]} \tag{6}$$

$$\frac{d[I_1]}{dt} = 0, \quad [I_1] = \frac{k_2[1][2]}{k_{-2} + k_3[3]} \tag{7}$$

We can now replace $[I_1]$ in the Eq. (6) to obtain this equation:

$$[I_2] = \frac{k_2 k_3[1][2][3]}{k_4[N^-][k_{-2} + k_3[3]]}$$

The value of $[I_2]$ can be put into Eq. (5) to obtain the rate Eq. (8) for the proposed mechanism:

$$rate = \frac{k_2 k_3 k_4[1][2][3][N^-]}{k_4[N^-][k_{-2} + k_3[3]]} \quad \text{or} \quad rate = \frac{k_2 k_3[1][2][3]}{[k_{-2} + k_3[3]]} \tag{8}$$

Since experimental data were indicated that steps 3 (k_3) and 4 (k_4) are fast but step 1 (k_2) is slow, it is therefore reasonable to make the following assumption:

$$K_3[3] >> k_{-2}$$

So the rate equation becomes:

$$rate = k_2[1][2] \tag{9}$$

This equation which was obtained from a mechanistic scheme (shown in Fig. 11) by applying the steady-state approximation

Table 12 The activation parameters involving $\Delta G^{\#}$, $\Delta S^{\#}$ and $\Delta H^{\#}$ for the reactions between (**1**, **2c** and **3**), (**1**, **2b** and **3**) and (**1**, **2a** and **3**) at 12.0 °C in 1, 2-dicholoroethane on the basis of Eyring equation.

Reaction	E_a(kJ/mol)	$\Delta G^{\#}$ (kJ.mol^{-1})	$\Delta H^{\#}$ (kJ.mol^{-1})	$\Delta S^{\#}$ (J.mol^{-1}.K^{-1})
1, **2c** and **3**	37.4	107.11	32.65	−261.10
1, **2b** and **3**	23.8	102.45	19.05	−292.46
1, **2a** and **3**	18.1	101.21	13.35	−308.09

is compatible with the results obtained by UV spectrophotometry. With respect to the Eq. (9) that shows the overall reaction rate (Fig. 1), the activation parameters involving $\Delta G^{\#}$, $\Delta S^{\#}$ and $\Delta H^{\#}$ for three reactions (**1**, **2a** and **3**, **1**, **2b** and **3** and also **1**, **2c** and **3**) could be now calculated by Eyring equation for the first step (rate determining step), as an elementary reaction, the results are reported in Table 12.

4. Further kinetic investigations

4.1. Effect of structure of dialkyl acetylenedicarboxylates

To confirm the above observations, further experiments were performed with diethyl acetylenedicarboxylate **2b** and dimethyl acetylenedicarboxylate **2a**, respectively, under the same conditions used in the previous experiments. As can be seen from Table 11 the behavior of diethyl acetylenedicarboxylate **2b** and dimethyl acetylenedicarboxylate **2a** is the same as for the di-*tert*-butyl acetylenedicarboxylate **2c** with respect to the reaction with triphenylphosphine **1** and 2-hydroxybenzimidazole **3**. The rate of the former reactions was also accelerated in a higher dielectric constant environment and with higher temperatures; however, these rates under the same condition are approximately 7–12.00 times more than reaction in the presence of di-*tert*-butyl acetylenedicarboxylate **2c** (Tables 11). It seems that both inductive and steric factors for the bulky alkyl groups in **2c** tend to reduce the overall reaction rate (see Eq. (9)). In the case of dimetyl acetylenedicarboxylate **2a**, the lower steric and inductive effects of the dimethyl groups exert a powerful effect on the rate of reaction.

5. Conclusions

The assignment of the *Z*- and *E*-isomers as a minor or major form in both the ylides **4a** and **4b** was undertaken by AIM and NPA methods and also CHelpG keyword. Quantum mechanical calculation was clarified how the ylides **4a** and **4b** exist in solution as a mixture of the two geometrical isomers. In addition the NMR study on the basis of theoretical calculations was employed for determination of chemical shifts and coupling constants of the two major *E*-**4**(**a, b**) and minor *Z*-**4**(**a, b**) geometrical isomers. These results were in good agreement with the experimental data. Furthermore, Kinetic investigation of these reactions was undertaken using UV spectrophotometry. The results can be summarized as follows: (**1**) the appropriate wavelengths and concentrations were determined to follow the reaction kinetics. (**2**) The overall reaction order followed second-order kinetics and the reaction orders with respect to triphenylphosphine, dialkyl acetylenedicarboxylate and 2-hydroxybenzimidazole were one, one and zero respectively. (**3**) The rates of all reactions were accelerated at higher temperatures. Under the same conditions, the activation energy of the reaction with di-*tert*-butyl acetylenedicarboxylate **2c** (37.4 kJ/mol) was higher than that for the both reactions which were followed by the diethyl acetylenedicarboxylate **2b** (23.8 kJ/mol) and dimethyl acetylenedicarboxylate **2a** (18.1 kJ/mol) in 1, 2-dichloroethane (**4**) The rates of all reactions were increased in solvents of higher dielectric constant and this can be related to differences in stabilization by the solvent of the reactants and the activated complex in the transition state. (**5**) Increased steric bulk in the alkyl groups of the dialkyl acetylenedicarboxylates, accompanied by the correspondingly greater inductive effect, reduced the overall reaction rate. (**6**) With respect to the experimental data, the first step in the proposed mechanism recognized as a rate-determining step (k_2) and this was confirmed based upon the steady-state approximation. (**7**) Also, the third step was identified as a fast step (k_3). (**8**) The activation parameters involving $\Delta G^{\#}$, $\Delta S^{\#}$ and $\Delta H^{\#}$ were reported using Eyring equation.

Acknowledgments

Authors sincerely thank the University of Sistan & Baluchestan and Payame Noor University for providing the financial support of this work.

References

Anary-Abbasineja, M., Anaraki-Ardakani, H., Hosseini-Mehdiaba, H., 2008. Phosphor. Sulfur Silicon Relat. Elem. 18, 1440.

Anaraki-Ardakan, H., Sadeghian, S., Rastegar, F., Hassanabadi, A., Anary-Abbasinejad, 2008. Syn. Commun. 38, 1990.

Arnol, W.D., Oldfield, E., 2000. J. Am. Chem. Soc. 122, 12835.

Aitken, R.A., Al-Awadi, N.A., Dawson, G., El-Dusouqui, O., Kaul, K., Kumar, A., 2007. Int. J. Chem. Kinet. 39, 6.

Bader, R.F.W., 1990. Atoms in Molecules: A Quantum Theory. Oxford University, New York.

Biegler Konig, F.W., Schönbohm, J., Bayle, D., 2001. J. Comput. Chem. 22, 545.

Crayson, M., Griffith, E.J., 1972. In: Topics in Phosphorus Chemistry, vol. 7. Insterscience, New York.

Cadogan, J.I.G., 1979. Organophosphorus Reagent in Organic Synthesis. Academic press, New York.

Dash, S.C., Das, N.N., Mohanty, P., 2011. Indian J. Chem. Technol. 18, 132.

Nielsen, O.J., Sehsted, J., Langer, S., Ljungström, E., Wängberg, I., 1995. Chem. Phys. Lett. 238, 359.

Engel, R., 1988. Synthesis of Carbon-phosphorus Bonds. CRC Press, Boca Rotan FL.

Fitjer, L., Quabeck, U., 1985. Synth. Commun. 15, 855.

Frisch, M. J., Trucks, G. W., Schlegel, H. B., Scuseria, G. E., Robb, M. A., Cheeseman, J. R., Zakrzewski, V. G., Montgomery, J. A., Stratmann, R. E., Burant, J. C., Dapprich, S, Millam, J. M., Daniels, A. D., Kudin, K. N., Strain, M. C., Farkas, O., Tomasi, J., Barone. V., Cossi, M., Cammi, R., Mennucci, B., Pomelli, C., Adamo, C., Clifford, S., Ochterski, J., Petersson, A., Ayala, P. Y., Cu, Q., Morokuma, K., Malick, D. K., Rabuck, A. D., Raghavachari, K., Foresman, J. B., Cioslowski, J., Ortiz, J. V., Baboul, A. G., Stefanov, B. B., Liu, G., Liashenko, A., Piskorz, P., Komaromi, I., Gomperts, R., Martin, R. L., Fox, D. J., Keith, T., Al-Laham, M. A., Peng, C. Y., Nanayakkara, A., Gonzalez, C., Challacombe, M., Gill, P. M. W., Johnson, B., Chen, W., Wong, M. W., Andres, J. L., Gonzalez, C., Head-Gordon, M., Replogle, E. S., Pople, J. A., 1998 GAUSSIAN98 Revision A.7 Pittsburgh Gaussian Inc.

Grabowsk, S.J., 2001. J. Mol. Struct. 562, 137.

Habibi-Khorassani, S.M., Maghsoodlou, M.T., Ebrahimi, A., Zakarianejad, M., Fattahi, M., 2007. J. Solution Chem. 36, 1117.

Habibi-khorassani, S.M., Ebrahimi, A., Maghsoodlou, M.T., Kazemian, M.A., Zakarianezhad, M., 2009. Phosphor. Sulfur Silicon Relat. Elem. 184, 2959.

Hudson, H.R., 1990. In: Hantley, F.R. (Ed.), Primary Secondary and Tertiary Phosphines, Polyphosphines and Heterocyclic Organophosphorus (III) Compounds in the Chemistry of Organophosphorus Compounds, vol. 1. Wiley, New York.

Hassanabad, A., Anary-Abbasinejad, M., Dehghan, A., 2009. Synth. Commun. 39, 132.

Islam, M.R., Hassani, Z., Saidi, K., 2003. Synth. Commun. 33, 65.

Islami, M.R., Mollazehi, F., Badiei, A., Sheibani, H., 2005. Arkivoc xv, 25.

Kalantari, M., Islami, M.R., Hassani, Z., Saidi, K., 2006. Arkivoc x, 55.

Maryanoff, B.E., Reit, A.B., 1989. Chem. Rev. 89, 863.

Maghsoodlou, M.T., Hazeri, N., Habibi-Khorassani, S.M., Moeeni, Z., Marandi, Gh., Lashkari, M., Ghasemzadeh, M., Bijanzadeh, H.R., 2007. J. Chem. Res., 566.

Maghsoodlou, M.T., Hazeri, N., Habibi-Khorassani, S.M., Ghulame-Shahzadeh, A., Nassiri, M., 2006a. Phosphor. Sulfur Silicon Relat. Elem. 18, 913.

Maghsoodlou, M.T., Heydari, R., Habibi-Khorassani, S.M., Rofouei, M.K., Nassiri, M., Mosaddegh, E., Hassankhani, A., 2006b. J. Sulfur Chem. 27, 341.

Okubo, T., Maeda, Y., Kitano, H., 1989. J. Phys. Chem. 93, 3721.

Rozas, I., Alkorta, I., Elguero, J., 2000. J. Am. Chem. Soc. 122, 11154.

Ramazan, A., Souldozi, A., 2005. Phosphorus Sulfur Silicon Relat. Elem. 180, 2801.

Ramazani, A., Bodaghi, A., 2000. Tetrahedron Lett. 41, 567.

Schwartz, L.M., Gelb, R.I., 1978. Anal. Chem. 50, 1592.

Wang, Z.G., Zhang, G.T., Guzei, I., Verkade, J.G., 2001. J. Org. Chem. 66, 3521.

Yavari, Adib M., Jahani-Mogaddam, F., Sayahi, M.H., 2002. Phosphor. Sulfur Silicon Relat. Elem. 177, 545.

Yavar, I., Alizadeh, A.A., 2003. Monatsh. Chem. 134, 435.

Yavari, I., Ali-Asgari, S., Porshamsian, K., Bagheri, M., 2007. J. Sulfur Chem. 28, 477.

Yavari, I., Hossain, Z., Alizadeh, A., 2006. Monatsh. Chem. 137, 1083.